

Multicamera Phase Measuring Profilometry For Accurate Depth Measurement

Yongchang Wang, Kai Liu, Qi Hao, Daniel Lau, Laurence G. Hassebrook
Electrical & Computer Engineering
A368 Astecc Building, University of Kentucky, Lexington, USA, 40506

ABSTRACT

Structured light illumination refers to a scanning process of projecting a series of patterns such that, when viewed from an angle, a camera is able to extract range information. Ultimately, resolution in depth is controlled by the number of patterns projected which, in turn, increases the total time that the target object must remain still. By adding a second camera sensor, it becomes possible to not only achieve wrap around scanning but also reduce the number of patterns needed to achieve a certain degree of depth resolution. But a second camera also makes it possible to reconstruct 3-D surfaces through stereo-vision techniques and triangulation between the cameras instead of between the cameras and the projectors. For both of these two tasks, correspondence between points from two cameras is essential. In this paper, we develop a new method to find the correspondence between the two cameras using both the phase information generated by the temporal multiplexed illumination patterns and stereo triangulation. We also analyze the resulting correspondence accuracy as a function of the number of structured patterns as well as the geometric position of projector to cameras.

Keywords: Structured light illumination, phase measuring profilometry, correspondence, stereo phase matching, sub-pixel.

1. INTRODUCTION

Structured light illumination (SLI) [1] employs the projection of a group of designed light patterns onto the surface of target. By the reflected illumination of the target, the depth information would be computed. The structured illumination could be spots, stripes or some other geometric patterns, as long as the depth information can be extracted from the reflected illumination. As one of the most accurate non-contact 3D surface measuring techniques, SLI has many industrial and scientific applications [1], including 3D conferencing [2], IC mounting on circuit board, and quality control [3]. Compared to some passive 3D information acquisition techniques such as stereo vision [19], shape from x [20], SLI can easily overcome the reconstruction ambiguities around surface discontinuities via the active scanning, and obtain accurate depth information through the camera-projector triangulation.

Among all SLI methods, the Phase Measuring Profilometry (PMP) is recognized as one of the most robust and precise strategy [5]. Multiple phase shift patterns are projected onto the 3D target and the depth data is extracted based on the phase distortion observed by the camera. The accuracy of the 3D surface relies on the quality of the 2D phase information. Compared to other SLI methods, PMP is known for its high accuracy, robustness to the environmental illumination and target texture, simple implementation, and fast point matching in 3D reconstruction. The goal of our research is to build a fast non-contact high-resolution 3D fingerprint scanner by using PMP technique. A multi-camera structured light illumination system is developed to improve the sensing resolution, neutralize the impact of lens distortion, reduce the illumination pattern number, and obtain the surrounding information of fingerprints.

Performing PMP scan with two cameras and one projector yields two 3D surfaces. We expect by fusing these two 3D surfaces to obtain a higher resolution, less distorted, and more wrapped version of 3D fingerprints. The key to merge reconstructed images from different cameras lies in finding the point correspondence among cameras. To illustrate the mismatching problem arisen in the point correspondence between two cameras in the system, a spots pattern has been designed and projected onto the finger under scanning.

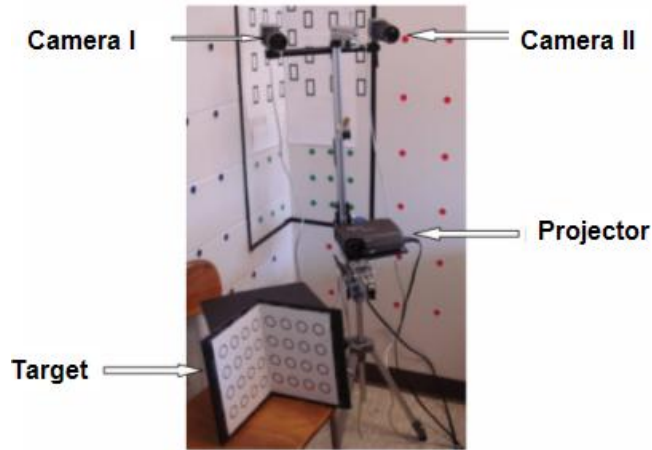


Figure 1.1: An experimental setup of the proposed 3D surface scanning system. The two 8 bit monochrome cameras used for depth scanner are Pulnix TM-1400CL, with 1392x1040 pixel resolution, interfaced with a PC with a Bitflow Roadrunner framegrabber card. The projector used is a Infocus Lp70+ with 1280x1024 pixel resolution and 1000 ANSI Lumens output.

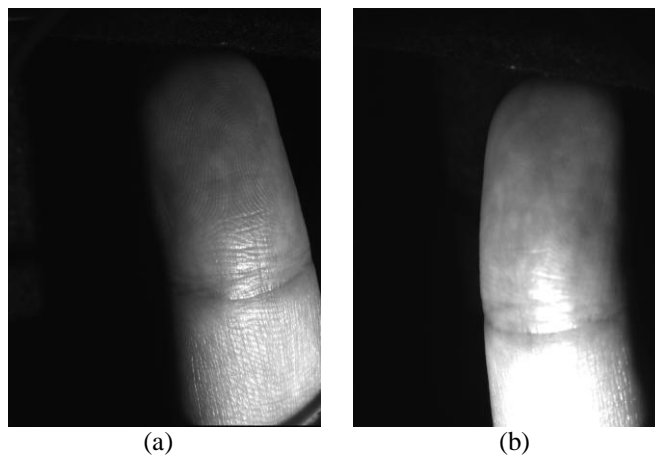


Figure 1.2: Two images from the camera I and camera II. (a) Camera I view; (b) Camera II view. Some part of the finger in each camera's field of view (FOV) is invisible in the other camera's FOV.

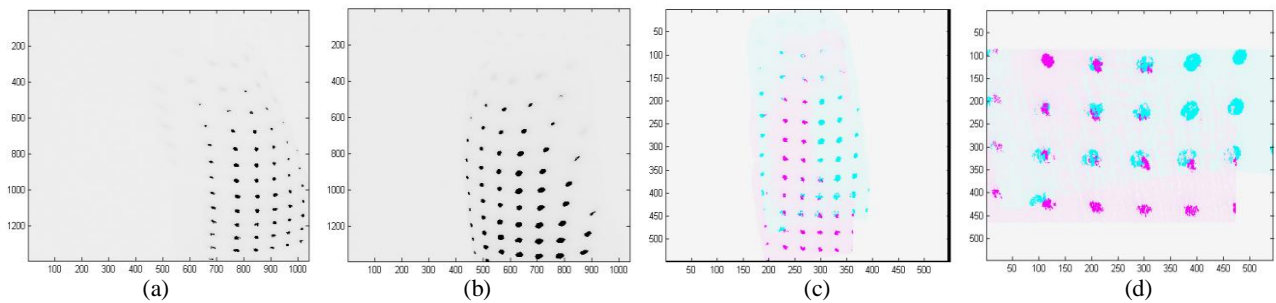


Figure 1.3: 3D surfaces after projecting the spots pattern onto the finger. Surfaces (a) and (b) are reconstructed from the camera I and II respectively. The spots are represented by the dark dots. Surface (c) is obtained by merging the surfaces (a) and (b) in 3D without any processing. Surface (d) is a zoomed part of the surface (c), which illustrates the mismatching of points.

The points mismatching, illustrated in figure 1.3, can be caused by many factors. Some of them are analyzed in [6] and [7]. A few remedying approaches have been proposed in [7], [8], and [9]. In a typical optical system, both cameras and projector will introduce distortions due to the curving lens surface and the limited aperture size. Using the PMP technique, the temporal multiplexed illumination patterns can offset the projector distortion, so the camera distortion remains the main cause of the mismatching. To overcome the multiple 3D surfaces mismatching caused by the distortion of camera lenses, we propose a method that can achieve the precise point correspondence between two 3D surfaces based on the notion of stereo vision.

Traditional stereo matching is to find the correspondence of points from two or more planes. Stereo matching has been studied for decades in computer vision, which can be broadly classified into feature based [10], [11], [12] and point based approaches [13] and [14]. Generally speaking, when come to two or more views geometry, the fundamental matrices and epipolar lines [15], [16] can be derived using an external calibration target. The corresponding points from different views must lie on the same epipolar line. That is, stereo matching greatly reduces the search for correspondences. The point correspondences deduce the stereo disparities. Through stereo triangulation, disparities can be converted into coordinates of points in 3D space.

In this paper, we present a new approach for 3D surface reconstruction with multiple cameras SLI systems by incorporating PMP technique into stereo vision correspondence. We employ epipolar geometry and sub-pixel technique to find the correspondence between phase images from different cameras and reconstruct the 3D surface. The system performance is further optimized by tuning three parameters: the alignment angle of patterns, the number of patterns, and the geometry among cameras and the projector. The optimized 3D surface reconstruction by our method is also compared with the performance of the conventional correlation based method.

2. PHASE MEASURING PROFILOMETRY

2.1 Traditional PMP process.

Traditional PMP projects either vertical or horizontal sine wave patterns onto the surfaces under scanning so that the vertical or horizontal correspondence information between the camera and the projector can be directly derived from the computed phase data. The canonical PMP technique employs single frequency sine wave patterns, shifted in turn, which can be described as

$$I_n(x^p, y^p) = A^p + B^p \cos(2\pi f y^p - 2\pi n/N) \quad (2.1.1)$$

where p represents the projection pattern, A^p and B^p are the projector constants, f is the frequency of the sine wave, and (x^p, y^p) represents one point in the projector coordinates. And the n is the phase shift index, less or equal to the total shifts number N . After projecting these patterns, the camera captures the image where the sine wave pattern is distorted by the scanned surface topology, and the resultant albedo image can be expressed as

$$I_n(x^c, y^c) = A^c(x^c, y^c) + B^c(x^c, y^c) \cos(\Phi(x^c, y^c) - 2\pi n/N) \quad (2.1.2)$$

where c represents the camera image, $\Phi(x^c, y^c)$ represents the phase information in the camera coordinates. After the projected pattern shifted by $2\pi/N$ for N times, the phase information $\Phi(x^c, y^c)$ at (x^c, y^c) can be retrieved by

$$\Phi(x^c, y^c) = \arctan \left[\frac{\sum_{n=1}^N I(x^c, y^c) \sin(2\pi n/N)}{\sum_{n=1}^N I(x^c, y^c) \cos(2\pi n/N)} \right] \quad (2.1.3)$$

As the phase value is linearly distributed in the projector coordinates, in the horizontal pattern case, y^p can be estimated from the phase data [17]. Then the 3D world coordinates of a point can be calculated with (x^c, y^c, y^p) . Figure 2.1 shows an 8-bit gray level phase image, which we will use in the later section for points matching.

2.2 Rotated structured illumination patterns:

We use patterns rotated in different angles to choose the optimal pattern alignment. Denote r as the alignment angle, L^p as the image length, and H^p as the image height. If we use single frequency patterns, then

$$f = 1/L^p \quad (2.2.1)$$

where L^p is the length of the pattern. If the pattern alignment is horizontal, *i.e.* $r = 0$, L^p is the height of the pattern. If the pattern alignment is vertical, *i.e.* $r = \pi/2$, L^p is the length of the pattern. In between,

$$\begin{aligned} L^p &= L^p / \sin(r) & \text{for } R < r < \pi/2 \\ L^p &= H^p / \cos(r) & \text{for } 0 < r \leq R \end{aligned}$$

where R is the arctan of the image length-to-height ratio. Thus, a rotated pattern with an angle r can be expressed as

$$I_n(x^p, y^p) = A^p + B^p \cos[2\pi f (\sin(r) y^p + \cos(r) x^p) - 2\pi n/N] \quad (2.2.3)$$

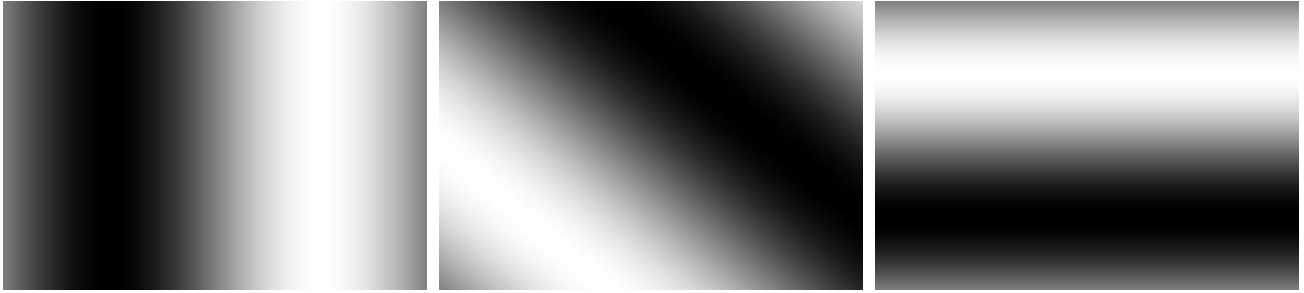


Figure 2.1: Three image patterns with different rotation angles. (a) shows the vertical pattern where $r = \pi/2$. (b), shows a pattern where $r = \pi/4$. (c) shows the horizontal pattern where $r = 0$.

2.3 Rotated phase image

From the camera point of view, the captured image is distorted by the scanned surface's topology. The function of reflected illumination can be described as

$$I_n(x^c, y^c) = A^c(x^c, y^c) + B^c(x^c, y^c) \cos[\Phi(x^c, y^c) - 2\pi n/N] \quad (2.3.1)$$

The computation of $\Phi(x^c, y^c)$ is similar as that of PMP, yet with an angle shift, denoted as θ , which is related to rotation angle r . It is given by

$$\Phi(x^c, y^c) = \left[\frac{\sum_{n=1}^N I(x^c, y^c) \sin(\theta + 2\pi n/N)}{\sum_{n=1}^N I(x^c, y^c) \cos(\theta + 2\pi n/N)} \right] \quad (2.3.2)$$

After converting $\Phi(x^c, y^c)$ from $0 \sim 2\pi$ to $0 \sim 255$, we can get the 8-bit gray level phase image.

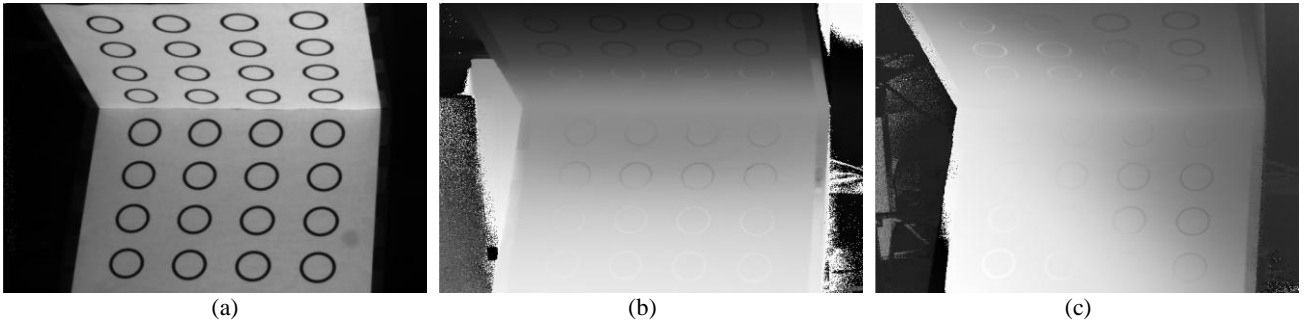


Figure 2.2: (a) The target image. (b) The phase image of the target when $r = 0$. (c) The phase image of the target when $r = \pi/4$.

The target shown in figure 2.2.a is used to evaluate the 3D reconstruction performance of the proposed rotated pattern PMP and sub-pixel stereo phase matching. Three pattern numbers in use, 25, 40 and 55, are for both traditional PMP and the rotated pattern PMP. Ten different angles are tested for each rotated pattern PMP. The results are given in figure 2.4. The reconstruction errors include the mean square root errors in x , y and z directions of the world coordinates in the unit of mm .

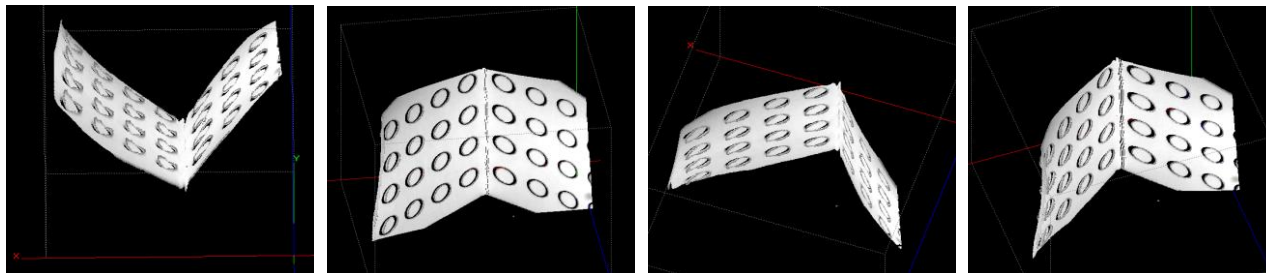


Figure 2.3: Images of the 3D reconstructed surface from four different perspectives using traditional PMP with 40 patterns.

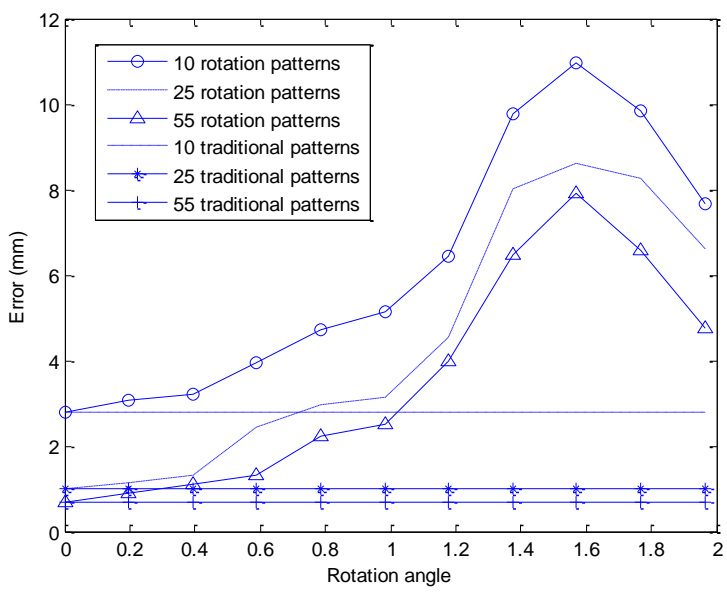


Figure 2.4: Plot of PMP reconstruction errors vs. rotation angles. The three straight lines are the errors of traditional PMP, where the pattern rotation angle is a constant.

Figure 2.3 shows the reconstructed surface of the target using traditional PMP technique with 55 patterns. Figure 2.4 shows the 3D reconstruction errors using rotated patterns in contrast to using traditional patterns, where the rotation angle is 0. With an increase of pattern number, the errors of 3D surface reconstruction drop as expected. For the rotation pattern PMP, the errors reach their maxima as the rotation angles go near $\pi/2$. This is because in our experimental system the camera-projector line is nearly vertical. Usually the best reconstruction results could be obtained when the pattern angle is perpendicular to the camera-projector line. In theory, when the pattern alignment is parallel to the camera-projector line, little information on y^p can be extracted, resulting in infinite reconstruction errors. In practice, as the camera and the projector are not perfectly vertically aligned, some information on y^p still can be derived even using vertical patterns. It also can be seen that when the number of patterns is larger than 25, there is no much room to improve the reconstruction performance.

3. STEREO MATCHING IN PHASE

3.1 Stereo vision geometry

Assume a real world point P projects to the two camera image planes as $p_1 (x^1, y^1, 1)$ and $p_2 (x^2, y^2, 1)$ respectively. Two matched points hold the following relation

$$p_1^T F p_2 = 0 \quad (3.1.1)$$

where F is the 3*3 Fundamental Matrix. If we expand equation 3.1.1, it becomes

$$(x^2 f_{11} + y^2 f_{12} + f_{13}) x^1 + (x^2 f_{21} + y^2 f_{22} + f_{23}) y^1 + (x^2 f_{31} + y^2 f_{32} + f_{33}) = 0 \quad (3.1.2)$$

which gives the explicit definition of epipolar lines. In other words, if the projected point p_2 in the image plane of camera II is known, we can derive the corresponding epipolar line in the image plane of camera I, on which the matched point p_1 lies.

To obtain the epipolar lines between the two cameras, we need to compute the Fundamental Matrix. The pre-known corresponding points are given by the calibration target shown in figure 2.2 a. Assume we have n pairs of matched points, denoted as $(x_1^1, y_1^1), \dots, (x_n^1, y_n^1)$ for the camera I and $(x_1^2, y_1^2), \dots, (x_n^2, y_n^2)$ from the camera II. Substitute all these points into equation 3.1.2, we can obtain

$$A f = 0 \quad (3.1.1)$$

where the n -by-9 matrix A is given by

$$A = \begin{bmatrix} x_1^2 x_1^1, y_1^2 x_1^1, x_1^1, x_1^2 y_1^1, y_1^2 y_1^1, y_1^1, x_1^2, y_1^2, 1 \\ x_2^2 x_2^1, y_2^2 x_2^1, x_2^1, x_2^2 y_2^1, y_2^2 y_2^1, y_2^1, x_2^2, y_2^2, 1 \\ \dots \\ x_n^2 x_n^1, y_n^2 x_n^1, x_n^1, x_n^2 y_n^1, y_n^2 y_n^1, y_n^1, x_n^2, y_n^2, 1 \end{bmatrix} \quad (3.1.2)$$

and n is the point pair number, chosen as 32 in our experiment. Vector f is defined as

$$f = [f_{11}, f_{12}, f_{13}, f_{21}, f_{22}, f_{23}, f_{31}, f_{32}, f_{33}]^T \quad (3.1.3)$$

The singular value decomposition (SVD) of A is denoted as

$$A = U \Sigma V^T \quad (3.1.4)$$

V^T 's last column is the null space of A , and hence is the vector F . In practice, F was computed using equation 3.1.2.

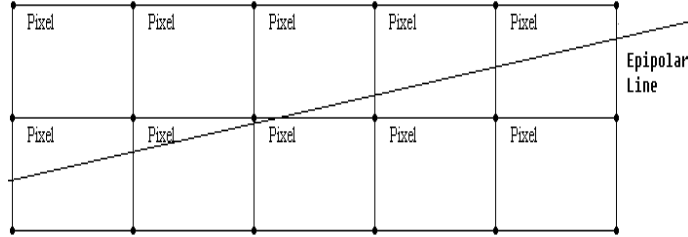


Figure 3.1: An illustration of a typical epipolar line and the neighboring pixels. Black dots represent the pixel vertices of an image. It can be seen that a real number valued epipolar line usually passes between the integer valued pixel vertices.

3.2 Stereo sub-pixel matching based on phase

The conventional pixel based stereo matching is to match an integer valued point $p_1 (x^1, y^1)$ in the image plane I to another integer valued point $p_2 (x^2, y^2)$ in the image plane II. Sub-pixel matching, by contrast, is to match an integer valued point p_1 to another real number valued point p_2' , to improve the matching accuracy and hence the 3D reconstruction resolution.

As shown in figure 3.2, we can model an epipolar line as

$$y = a x + b \quad (3.2.1)$$

If the coordinate of p_1 is (i, j) , the coordinate of p_2 on the epipolar line would be $(i+h, j+l)$. Equation 3.2.1 can be rewritten as

$$(j+l) = a (i+h) + b$$

Let $a' = 1/a$ and $b' = (j-b -a)$, it would be

$$h = a' l + b' \quad (3.2.2)$$

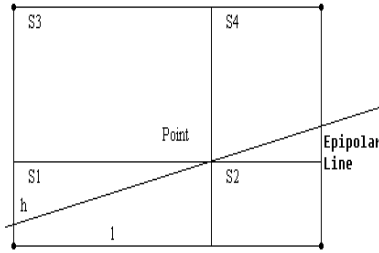


Figure 3.2: An epipolar line goes through the space between four image pixel centers. The real number valued matched point on the epipolar line divides the space into 4 rectangular regions, with normalized areas of S_1 , S_2 , S_3 , and S_4 , as $S_1 + S_2 + S_3 + S_4 = 1$.

If we assume that the phase value inside each square is linear, to compute the phase value of each point on the epipolar line, we have

$$P = s_1 p_4 + s_2 p_3 + s_3 p_2 + s_4 p_1 \quad (3.2.3)$$

where P is the phase value of the point on the epipolar line. p_1 , p_2 , p_3 , and p_4 are the phase values of the four integer indexed pixels. From figure 3.2, we can describe the four rectangle areas as:

$$s_1 = l h$$

$$s_2 = (1-l) h$$

$$s_3 = l(1-h)$$

$$s_4 = (1-l)(1-h) \quad (3.2.4)$$

Substitute equation 3.2.3 into 3.2.2, we can describe the phase value as

$$P = p_1' l h + p_2' h + p_3' l + p_4' \quad (3.2.5)$$

where $p_1' = p_4 - p_3 - p_2 + p_1$, $p_2' = p_3 - p_1$, $p_3' = p_2 - p_1$ and $p_4' = p_1$. Combined with equation 3.2.1, it turns out to be

$$P = p_1' a' l^2 + (p_1' b' + p_2' a' + p_3')l + (p_2' b' + p_4') \quad (3.2.6)$$

As a result, to find the point on the epipolar line with the phase value P amounts to solving the quadric function of 3.2.5.

3.3 Reconstruction of 3D surface

3D reconstruction from multiple images has been given in [16] and [18]. After the correspondences between the visible points from the two camera images is built by the approach described in section 3.2. We use the linear camera model to reconstruct the 3D surfaces.

The transformation equations from real world to camera is given by

$$x^c = \frac{m_{11}^{wc} x^w + m_{12}^{wc} y^w + m_{13}^{wc} z^w + m_{14}^{wc}}{m_{31}^{wc} x^w + m_{32}^{wc} y^w + m_{33}^{wc} z^w + m_{34}^{wc}}$$

$$y^c = \frac{m_{21}^{wc} x^w + m_{22}^{wc} y^w + m_{23}^{wc} z^w + m_{24}^{wc}}{m_{31}^{wc} x^w + m_{32}^{wc} y^w + m_{33}^{wc} z^w + m_{34}^{wc}} \quad (3.3.1)$$

where m_{ij}^{wc} is the parameter of world-to-camera matrix M^{wc} , which is calculated from camera calibration,

$$M^{wc} = \begin{bmatrix} m_{11}^{wc} & m_{12}^{wc} & m_{13}^{wc} & m_{14}^{wc} \\ m_{21}^{wc} & m_{22}^{wc} & m_{23}^{wc} & m_{24}^{wc} \\ m_{31}^{wc} & m_{32}^{wc} & m_{33}^{wc} & m_{34}^{wc} \end{bmatrix} \quad (3.3.2)$$

Denote M^{wc1} as the world-to-camera matrix of the camera I, and M^{wc2} for the camera II. For a 3D point, the relation between its world coordinates (x^w, y^w, z^w) and its projection coordinates (x^{c1}, y^{c1}) and (x^{c2}, y^{c2}) can be described as $Q [x^w, y^w, z^w]^T = R$, that is

$$\begin{bmatrix} m_{31}^{wc1} x^{c1} - m_{11}^{wc1}, m_{32}^{wc1} x^{c1} - m_{12}^{wc1}, m_{33}^{wc1} x^{c1} - m_{13}^{wc1} \\ m_{31}^{wc1} y^{c1} - m_{21}^{wc1}, m_{32}^{wc1} y^{c1} - m_{22}^{wc1}, m_{33}^{wc1} y^{c1} - m_{23}^{wc1} \\ m_{31}^{wc2} x^{c2} - m_{11}^{wc2}, m_{32}^{wc2} x^{c2} - m_{12}^{wc2}, m_{33}^{wc2} x^{c2} - m_{13}^{wc2} \\ m_{31}^{wc2} y^{c2} - m_{21}^{wc2}, m_{32}^{wc2} y^{c2} - m_{22}^{wc2}, m_{33}^{wc2} y^{c2} - m_{23}^{wc2} \end{bmatrix} [x^w, y^w, z^w]^T = \begin{bmatrix} m_{14}^{wc1} - m_{34}^{wc1} \\ m_{24}^{wc1} - m_{34}^{wc1} \\ m_{14}^{wc2} - m_{34}^{wc2} \\ m_{24}^{wc2} - m_{34}^{wc2} \end{bmatrix} \quad (3.3.3)$$

The pseudo-inverse solution can be derived as

$$[x^w, y^w, z^w]^T = (Q^T Q)^{-1} Q^T R \quad (3.3.4)$$

The target shown in figure 2.2.a was used again to test the 3D reconstruction errors of the proposed sub-pixel stereo phase matching technique. We used ten different rotation angles. For each rotation angle, three different pattern numbers, 55, 25 and 10, were chosen. The errors of matching point pair estimation are measured in mean square root error of x (vertical) and y (horizontal) directions of image coordinates.

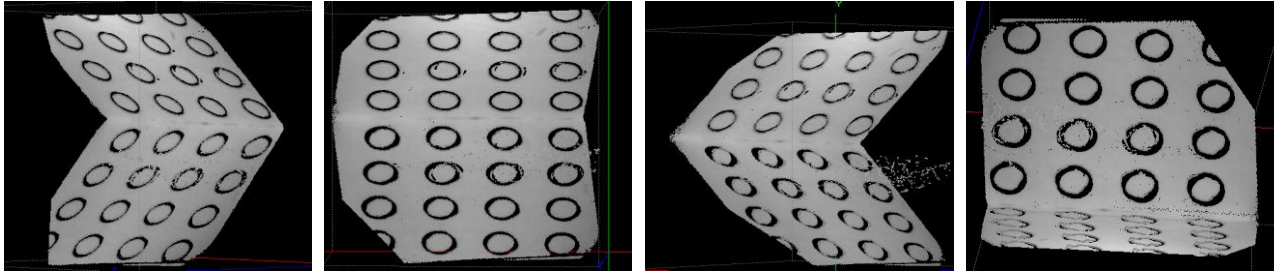


Figure 3.3: Sub-pixel stereo phase matching reconstruction with 55 vertical patterns. Images from left to right are four different views of this 3D surface.

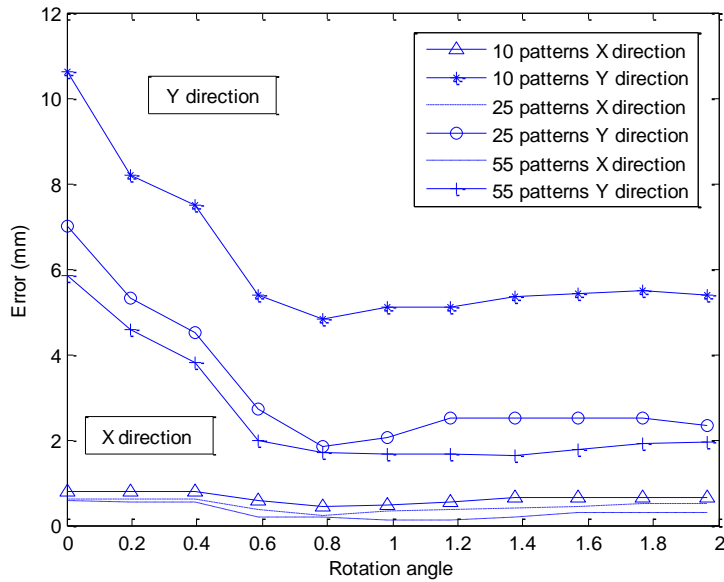


Figure 3.4: Reconstruction errors using sub-pixel stereo phase matching vs. the rotation angles. The upper three curves are errors in y direction. The lower three curves are the errors in x direction.

The performance of sub-pixel stereo phase matching depends on both the quality of phase information and the angle between pattern alignment and epipolar lines. If the pattern alignment is parallel to one epipolar line, all the points on this line will have the same phase value; in that case, the stereo matching by phase becomes impossible. In our prototype system, the two cameras are positioned horizontally; therefore the vertical patterns should yield the best reconstruction results. However, figure 3.4 shows that the best results happen at the rotation angle of near 0.8, instead of $\pi/2$. That is because the reconstruction performance also relies on the quality of phase information. As figure 2.4 shows, the quality of phase information, equivalent to depth errors, degrades most when the pattern alignment goes near $\pi/2$. Besides, there is an angle between the alignments of two cameras, which can not generate a set of parallel horizontal epipolar lines as expected.

It can also be seen from figure 3.4 that the error in x direction (vertical) is much less than those in y direction (horizontal). Since the epipolar lines are near horizontal, such a stereo vision geometry helps reduce the errors in x direction. In addition, although the phase information degrades most when the pattern rotation angle goes near $\pi/2$ as shown in figure 2.4, the sub-pixel stereo matching reconstruction, even in y direction, does not degrade as much as conventional PMP reconstruction does. It seems that the proposed sub-pixel stereo matching is quite robust to the quality of the phase information extracted using the PMP technique.

4. CAMERA-PROJECTOR GEOMETRY OPTIMIZATION

Sub-pixel stereo matching in phase with vertical patterns and three pattern numbers, 15, 30, and 60, are applied in optimizing the camera-projector-camera geometry. The matching error is defined as the mean square root error between the actual matching points and the estimated matching points of the target images. To obtain better phase information, multi-frequency patterns were used [17]. Three frequencies were chosen as 1, 8, and 32.

Figure 4.1 shows the geometry of the system setup. Figure 4.2 illustrates the point matching errors vs. $\log(H/L)$. The mean square root errors in x and y directions using multi-frequency patterns are reduced, compared to the case of using single frequency patterns, as the quality of phase information is much improved by using multiple frequencies patterns. As shown in figure 4.2, the matching errors drop as the log ratio of H/L decreases. It suggests that the best position of the projector is the middle point of two cameras.

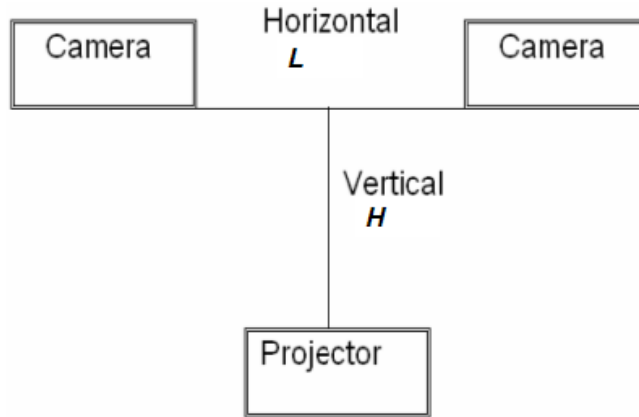


Figure 4.1: Geometry of camera-projector-camera triangle. The distance between two cameras is defined as L , which is fixed in our experiment. H is defined as the distance between the projector and the middle point of two cameras.

Figure 4.3 shows the reconstruction results of the target by the proposed sub-pixel phase based stereo matching and the conventional correlation based stereo matching. For the proposed method, the errors are 0.1485 pixels in x direction and 0.5833 in y direction. For the conventional method, the errors are 1.5293 pixels in x direction and 15.4825 pixels in y direction. Compared to the traditional stereo matching, the results of sub-pixel stereo phase matching are more accurate and more robust to noise. While traditional correlation based stereo matching may achieve higher quality reconstruction for objects with rich texture information, the proposed phase based stereo matching approach can effectively reconstruct 3D surfaces under all the texture and illumination conditions.

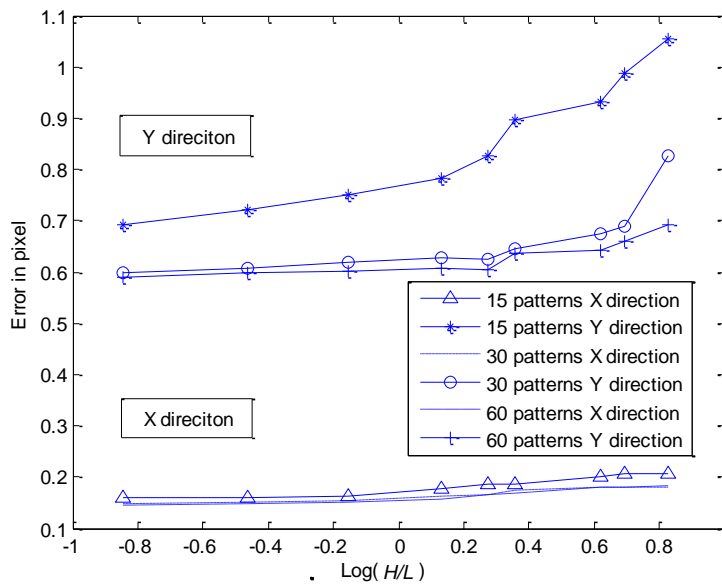


Figure 4.2: Matching errors in pixel vs. log ratio of H/L . The upper three curves are the errors in y direction. The lower three curves are the errors in x direction.

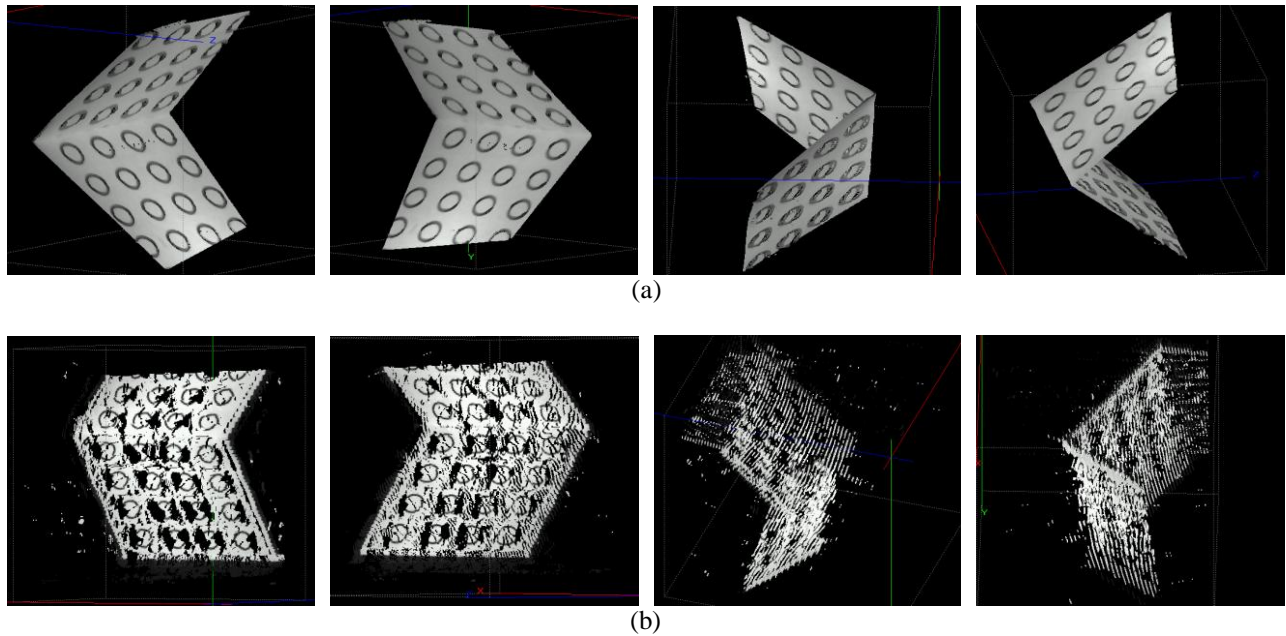


Figure 4.3: (a) Surfaces reconstructed by sub-pixel stereo matching, with 3 frequencies of 1, 8, and 32, 10 patterns for each frequency. (b) Surfaces reconstructed by traditional correlation based stereo matching.

5. CONCLUSION AND FUTURE RESEARCH

In this paper, we propose a phase information based sub-pixel stereo matching for multi-perspective structured light illumination 3D surface reconstruction. We also investigate the impact of pattern rotation angles, pattern numbers, and camera-projector-camera geometry on the reconstruction performance. The advantages of using multiple cameras in SLI scanning over the single camera SLI system include its higher robustness to the quality of phase information, as well as the measurement noise, and its capability to acquire surrounding information of objects under examination. Compared to the traditional correlation based stereo matching, the proposed method can produce high quality 3D surface reconstruction despite the texture and illumination conditions. Our future work includes applying such a technique to 3D face and 3D finger/palm print reconstruction.

REFERENCES

1. J. Salvi, J. Pages, J. Batlle, "Pattern codification strategies in structured light systems", *Pattern Recognition*, 37(4), April 2004.
2. G. Schmaltz of Schmaltz Brothers Laboratories, "A method for presenting the profile curves of rough surfaces", *Naturwiss*, 18, 315-316, March 9 1932.
3. Ramesh Raskar, Greg Welch, Matt Cutts, Adam Lake, Lev Stesin, Henry Fuchs, "The office of the future: a unified approach to image-based modeling and specially immersive displays", *SIGGRAPH 98*, Orlando, Florida, July 19-24, 1998.
4. T.S Newman, "A survey of automated visual inspection", *Image Understanding*, 61, 231-262, 1995.

5. V. Srinivasan, H.C. Liu, M. Halioua, "Automated phase-measuring profilometry of 3D diffuse objects", *Applied Optics*, 23(18), 3105-3108, 1984.
6. Faugeras, O. D. & Toscani, G. (1987) Camera calibration for 3D computer vision. Proc. uInternational Workshop on Industrial Application of Machine Vision and Machine Intelligence, Silken, Japan, p. 240-247.
7. Melen, T.(1994) "Geometrical modeling and calibration of video cameras for underwater navigation". Dr. ing thesis, Norges tekniske hogaskole, Institutt for teknisk bybernetikk.
8. Wei, G. Q. & Ma, S. D. (1993) "A complete two-plane camera calibration method and experimental comparisons". Proc. 4th International Conference on Computer Vision, Berlin, Germany, p. 439-446.
9. Weng, J., Cohen, P. & Herniou, M. (1992) "Camera calibration with distortion models and accuracy evaluation". *IEEE Transactions on Pattern Analysis and Machine Intelligence PAMI-14(10)*: 965-980.
10. U. Dhond and J. Aggarwal, "Structure from Stereo - A Review", *IEEE Trans. Syst., Man and Cybern.* 19, 1489-1510, 1989.
11. T. Moons, L. Van Gool, M. Proesmans and E. Pauwels, "Affine reconstruction from perspective image pairs with a relative object-camera translation in between", *IEEE Transactions on Pattern Analysis and Machine Intelligence*, vol. 18, no.1, pp. 77-83, Jan. 1996.
12. S. Pollard, J. Mayhew and J. Frisby, "PMF: A Stereo Correspondence Algorithm Using a Disparity Gradient Limit", *Perception* 14(4), 449-470, 1985.
13. M. Okutomi and T. Kanade, "A Locally Adaptive Window for Signal Processing", *International Journal of Computer Vision*, 7, 143-162, 1992.
14. I. Cox, S. Hingorani and S. Rao, "A Maximum Likelihood Stereo Algorithm", *Computer Vision and Image Understanding*, Vol. 63, No. 3, May 1996.
15. R. Hartley, R. Gupta, and T. Chang. "Stereo from uncalibrated cameras", *Proceedings of the Conference on Computer Vision and Pattern Recognition*, pages 761-764, Urbana-Champaign, Illinois, 1992.
16. O. Faugeras. "What can be seen in three dimensions from an uncalibrated stereo rig?", *Proceedings of the 2nd European Conference on Computer Vision*, pages 563-578, Santa Margherita Ligure, Italy, 1992. Springer-Verlag.
17. Veeraganesh Yalla, L.G. Hassebrook, "Very High Resolution 3D Surface Scanning Using Multi-frequency Phase Measuring Profilometry", *Spaceborne Sensors II, SPIE's Defense and Security Symposium*, Vol. 5798-09, 2005.
18. O. Faugeras, "Three-Dimensional Computer Vision - A Geometric Viewpoint", *Artificial intelligence*. M.I.T. Press, Cambridge, MA, 1993.
19. S.D. Cochran and G. Medioni, "3D surface description from binocular stereo", *IEEE PAMI*, 14(10), 981-994, 1992.
20. P. Tsai and M. Shah, "Shape from shading with variable albedo", *Opt. Eng.* 37(4), 1212-1220, 1998.